Sparse SAR Tomography of Ice Sheet and Bed

Anton Heister, German Aerospace Center (DLR), Microwaves and Radar Institute, anton.heister@dlr.de, Germany
Rolf Scheiber, German Aerospace Center (DLR), Microwaves and Radar Institute, rolf.scheiber@dlr.de, Germany

Abstract

Modern radars for radio-echo sounding of ice sheets carry multiple receive channels in cross-track, allowing for clutter suppression, as well as for synthetic aperture radar tomography of the ice sheet and bed. Tomographic processing provides 3-D information about the sub-surface topography, bed conditions and internal layers' orientation. We explore synthetic aperture radar tomography based on sparse signal reconstruction, offer a particular algorithm implementation and demonstrate its performance using data acquired by the Multichannel Coherent Radar Depth Sounder of the Center for Remote Control of Ice Sheets during the 2008 campaign in Greenland.

1 Introduction

The ability to estimate ice sheet mass balance and dynamics requires knowledge of ice-sheet thickness, basal topography and its roughness, bed conditions, internal layers' geometry, surface topography and velocity [1]. An additional requirement for improved ice sheet mass balance modeling is the availability of the aforementioned data in high resolution and with wide spatial coverage [2].

Synthetic aperture radar (SAR) tomography is a technique, providing radio-echo sounding (RES) radars with a capability of a 3-D imaging, which, compared to a conventional 2-D nadir-looking mode, increases the coverage in the cross-track direction, and depending on a particular processing strategy, may also improve image resolution in cross-track.

For conventional processing, the cross-track resolution is proportional to the system's wavelength and inversely proportional to the cross-track baseline [3]. The fact, that the most commonly used wavelength range for RES of ice sheets is $\lambda \in [1, 10]\mathrm{m}$, makes it unfeasible to create large cross-track baselines both for airborne and spaceborne missions. The use of advanced processing approaches is therefore needed to overcome the aforementioned limitation [4].

In this paper we extend our previous work on sparse SAR tomography of the ice sheet and bed [5], which used a point target assumption, by including usage of a sparsifying transformation. We evaluate the performance using a dataset containing six cross-track channels, provided by the Center for Remote Control of Ice Sheets (CReSIS), Kansas, USA [6].

2 Problem Formulation

In this paper we assume that the ice sheet consists of the ice surface and the bed, with internal layers possibly present in between. Cross-track RES geometry and a typical cross-track power distribution profile for a particular range bin are shown in Fig. 1, where for the sake of simplicity we ignore the ray-bending effect due to the variation of the media's electrical permittivity during the propagation of the electromagnetic wave.

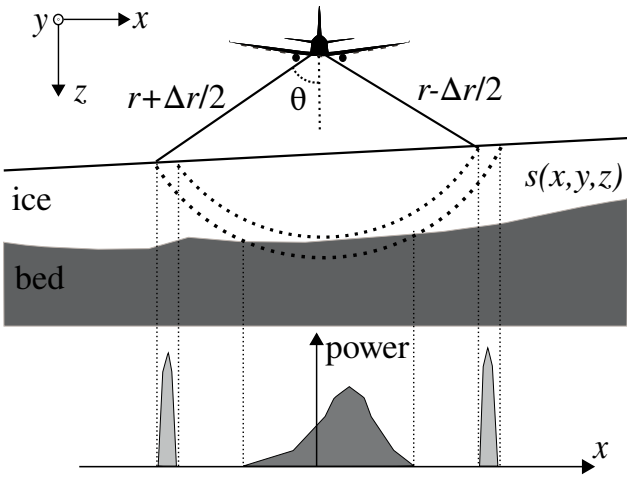

Figure 1: Cross-track imaging geometry

Finding an unknown complex reflectivity of the scene $s(x, y, z)$ is typically done separately for each dimension. Firstly, range compression is performed using matched filtering; secondly, azimuth compression is performed using SAR processing that takes along-track ray-bending into account. After that SAR echograms for each of the M cross-track channels are calibrated and equalized. Lastly, cross-track processing is carried out. Making an assumption that azimuth compression has a δ-function impulse response, the received signal for a particular range bin r for a cross-track channel $m = (1, M)$ can be mathematically expressed as follows:

$$g_m = \int_{I_\theta} \int_{I_r} s(r, \theta) \exp(-j\pi\xi_m r \sin\theta) dr d\theta + w_m, \quad (1)$$

where the integration limits in range are defined by the range resolution Δr and lie in the interval $I_r \in [r - \Delta r/2, r + \Delta r/2]$; the integration limits in cross-track are

ISBN 978-3-8007-4636-1 / ISSN 2197-4403

defined by the beamwidth of the antenna pattern in cross-track $\Delta\theta$ and lie in the interval $I_\theta \in [-\Delta\theta/2, \Delta\theta/2]$; $\xi_m = -2x_m/(\lambda r)$ is the cross-track wavenumber component with x_m being a cross-track baseline of the m-th receive channel, and λ being the wavelength of the transmitted wave in vacuum; w_m is noise.
By discretizing (1) we get a system of M linear equations

$$\mathbf{g} = \mathbf{A}\mathbf{s} + \mathbf{w}, \tag{2}$$

where $\mathbf{g} \in \mathbb{C}^M$ is the received signal vector, $\mathbf{A} \in \mathbb{C}^{M,N}$ is a sampling matrix whose columns contain steering vectors $\mathbf{a}_n = -2\pi\mathbf{x}\sin\theta_n/\lambda$, N is a number of cross-track incidence angles after discretization, $\mathbf{s} \in \mathbb{C}^N$ is an unknown complex reflectivity vector, $\mathbf{w} \in \mathbb{C}^M$ is noise.

3 Sparse SAR Tomography

In the real case scenario $M \ll N$, meaning that the inversion of (2) is ill-posed, and there exist infinitely many solutions. Sparse reconstruction, also known as compressed sensing (CS) [7], is a signal processing approach that allows for a correct reconstruction of signals sampled at a rate significantly below Nyquist rate, if two requirements are met. First, the solution is known to be sparse in some domain, i.e. there exists a basis $\mathbf{\Psi} \in \mathbb{C}^{N,N}$ such that $\boldsymbol{\gamma} = \mathbf{\Psi}\mathbf{s}$ has at most $K \ll N$ nonzero elements. Second, the columns of the sampling matrix $\mathbf{A}$ satisfy restricted isometry property [7], which defines a tolerable level of their mutual coherency. We rewrite (2) in terms of CS framework as following

$$\mathbf{g} = \mathbf{A}\mathbf{\Psi}^{-1}\boldsymbol{\gamma} + \mathbf{w} = \mathbf{\Phi}\boldsymbol{\gamma} + \mathbf{w}. \tag{3}$$

One particular CS implementation, that uses the multiple measurement vector (MMV) model and the joint sparsity [8] assumption, is of a great interest to us, as it relaxes the incoherence requirement for the columns of $\mathbf{A}$, which in our case is predetermined by the cross-track channels' geometry x_m. In terms of RES of the ice-sheet and bed, the assumptions of [8] translate into a requirement that ice-sheets and bed topography varies slowly in azimuth. We rewrite (3) using the MMV model as follows:

$$\mathbf{G} = \mathbf{A}\mathbf{\Psi}^{-1}\mathbf{\Gamma} + \mathbf{W} = \mathbf{\Phi}\mathbf{\Gamma} + \mathbf{W}, \tag{4}$$

where $\mathbf{G} \in \mathbb{C}^{M,L}$, $\mathbf{\Gamma} \in \mathbb{C}^{N,L}$, $\mathbf{W} \in \mathbb{C}^{M,L}$, L is a number of azimuthal samples.
There are several effective algorithms for solving the MMV problem (4). In this paper we use the MMV focal underdetermined system solver (M-FOCUSS) [9], which uses the iteratively reweighted least squares method to minimize the so-called p-q norm-like diversity measure of an unknown MMV matrix $\mathbf{\Gamma}$

$$J(\mathbf{\Gamma})^{(p,q)} = \sum_{i=1}^{L} (\|\mathbf{\Gamma}[i]\|_q)^p, 0 \leqslant p \leqslant 1, q \geqslant 1, \tag{5}$$

where for this paper we take $p = 0.8$ and $q = 2$.

The M-FOCUSS algorithm is summarized as follows:

Require: $\mathbf{G}$, $\mathbf{\Phi}$, p, q, regularization parameter α
Ensure: sparse coefficients matrix $\mathbf{C}$
1: initialize $\mathbf{C}_0 = \mathbf{I}$, $\mathbf{\Phi}_0 = \mathbf{\Phi}$, $i = 1$
2: **while** stopping condition is not met **do**
3: $\quad\widetilde{\mathbf{W}}_i \leftarrow \mathrm{diag}(p^{-1/2}\,\|c_{i-1}\|_q^{1-p/2})$
4: $\quad\mathbf{\Phi}_i \leftarrow \mathbf{\Phi}_{i-1}\widetilde{\mathbf{W}}_i$
5: $\quad\mathbf{C}_i \leftarrow \widetilde{\mathbf{W}}_i\mathbf{\Phi}_i^H(\mathbf{\Phi}_i\mathbf{\Phi}_i^H + \alpha\mathbf{I})^{-1}\mathbf{G}$
6: $\quad i \leftarrow i + 1$
7: **end while**
8: **return** $\mathbf{C}_i$

The computational complexity of M-FOCUSS is determined by steps 4 and 5, whose complexity is respectively $\mathcal{O}(N^2M)$ and $\mathcal{O}(N^3)$ [10]. In case of high and moderate SNR the regularization parameter α is constant for each iteration and is fixed to the noise power σ^2. For further processing we take $N = 91$ with uniformly sampled cross-track incidence angle lying in the interval $\theta_n \in [-45°, 45°]$, and $L = 21$ which corresponds to the platform's azimuth displacement of $\Delta y = 30\,\mathrm{m}$.

4 Experimental Results

In order to demonstrate the performance of M-FOCUSS for SAR tomography of the ice-sheet and bed, we process data collected by the CReSIS's MCoRDS system. We selected a $28\,\mathrm{km}$ track flown over south-east Greenland. The region of the study and the track's trajectory are shown in Fig. 2, parameters of the system and the acquisition are summarized in Table 1. The system has six receiving channels with cross-track spacing $\mathbf{x}^{\mathrm{T}} = [-2.40, -1.41, -0.47, 0.48, 1.42, -2.39]\,\mathrm{m}$.

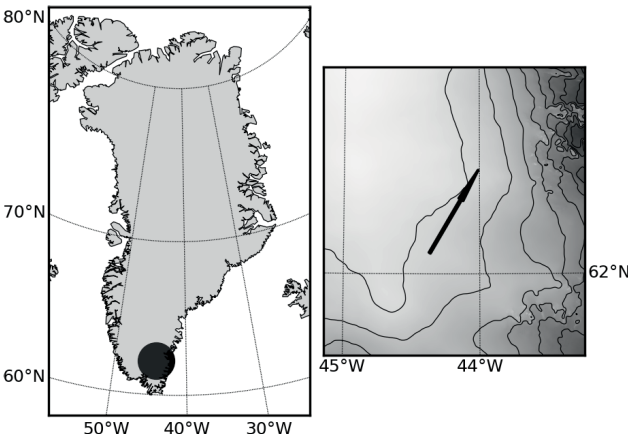

Figure 2: MCoRDS datatake on a map. The map of Greenland is plotted using a stereographic projection with a central meridian of 41° W and a central parallel of 72° N. Isolines on the track's map correspond to a surface elevation change of 250 m.

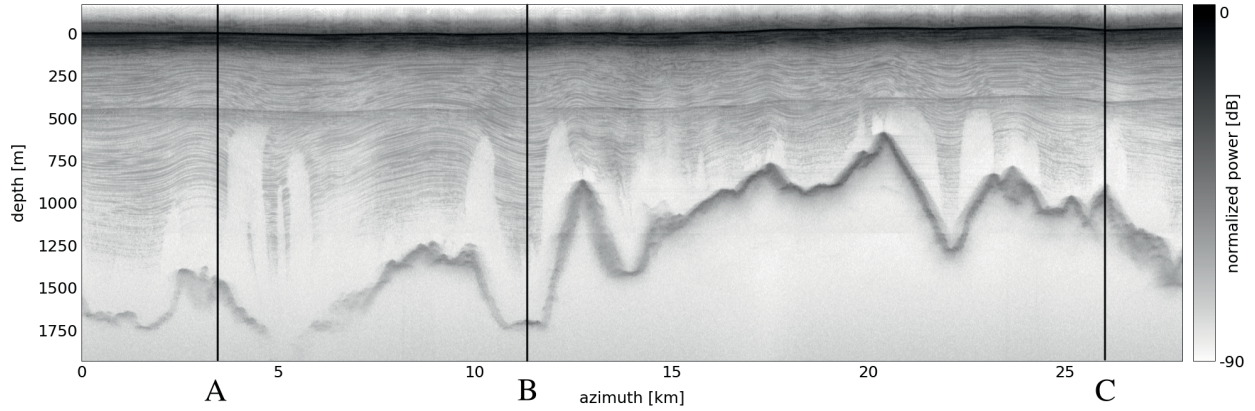

Figure 3: SAR echogram with conventional beamforming applied.

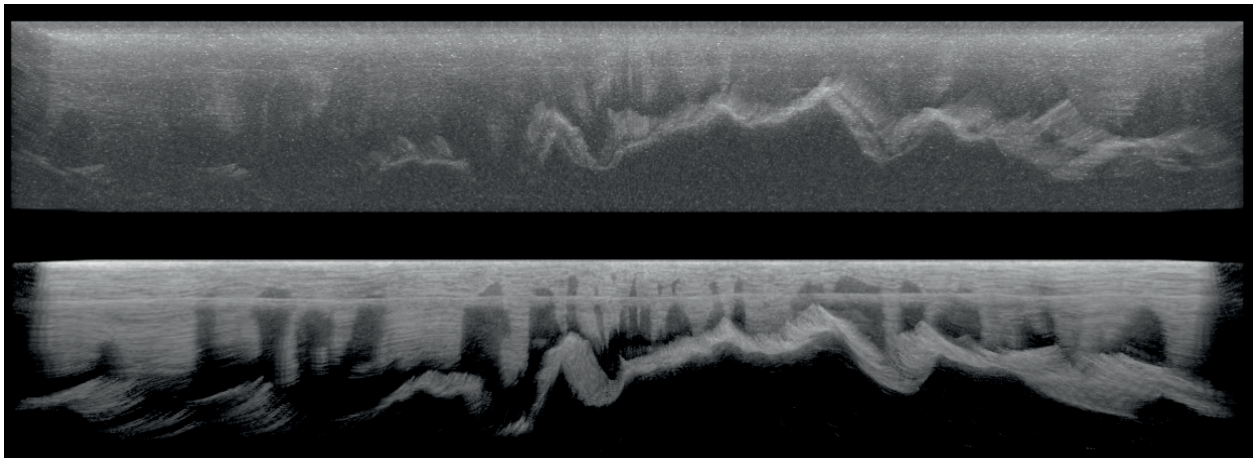

Figure 4: Comparison of rendered volumetric images. The image on top was processed using MVDR, the image on the bottom was processed using M-FOCUSS.

Parameters	Value
Central frequency	150 MHz
Chirp bandwidth	20 MHz
Chirp duration	$3/10\,\mu$s
Sampling frequency	120 MHz
Effective PRF	156 Hz
Number of cross-track channels	6
Effective cross-track aperture	4.79 m
Acquisition date	2008-08-01
Acquisition start UTC	16:54:42
Acquisition end UTC	17:02:59
Average height above the ice surface	800 m

Table 1: Parameters of MCoRDS acquisition.

The choice of a proper sparsifying basis $\mathbf{\Psi}$ plays a key role in achieving good reconstruction quality in CS. For this paper we chose symmetric biorthogonal wavelets. We note however, that the ice-sheet surface, internal layers and the bed all have different backscattering characteristics, which is mainly explained by the difference in the features' roughness and materials. Therefore it is most likely that a single wavelet basis will not be optimal for SAR tomography of the ice-sheet, and an additional study is needed to find the optimal basis. A technique that allows to analyze along-track angular backscattering characteristics of ice-sheets, such as the one offered in [11], can be used to train the optimal dictionary.

We select three azimuthal positions, as shown on the track's echogram in Fig. 3. The bed has a negative cross-track slope at position $A \approx 3.5\,\mathrm{km}$, is straight at position $B \approx 11.5\,\mathrm{km}$, and has a positive cross-track slope at position $C \approx 26\,\mathrm{km}$. For each chosen azimuthal position we compare results of SAR tomography using M-FOCUSS and minimum variance distortionless response (MVDR) estimator in Fig. 5. We plot the images in Cartesian coordinates, where during the coordinate transformation the ray-bending in cross-track is taken into account.

We see a positive correlation between the orientation of the bed and internal layers in Fig. 5. The internal layers' response is specular, prominent only at a narrow range of x, whereas the bed response is wide. The surface multiple is also present at depth $d \approx 500\,\mathrm{m}$, where its con-

ISBN 978-3-8007-4636-1 / ISSN 2197-4403

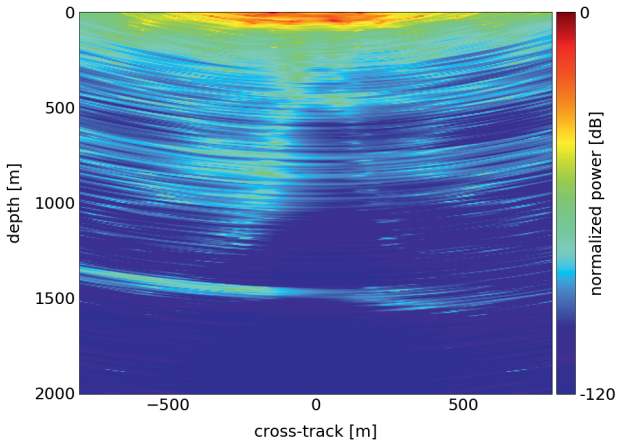

(a) MVDR, A

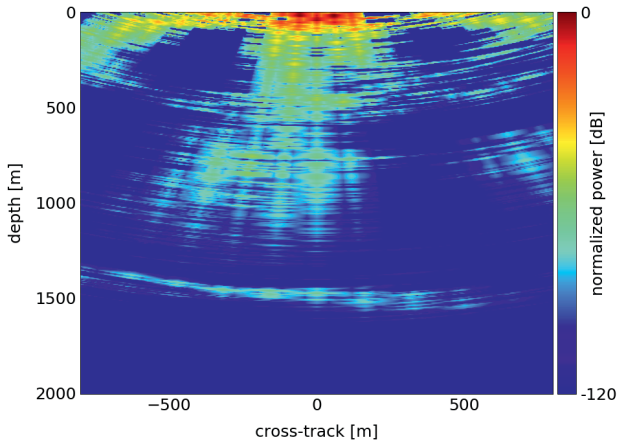

(b) M-FOCUSS, A

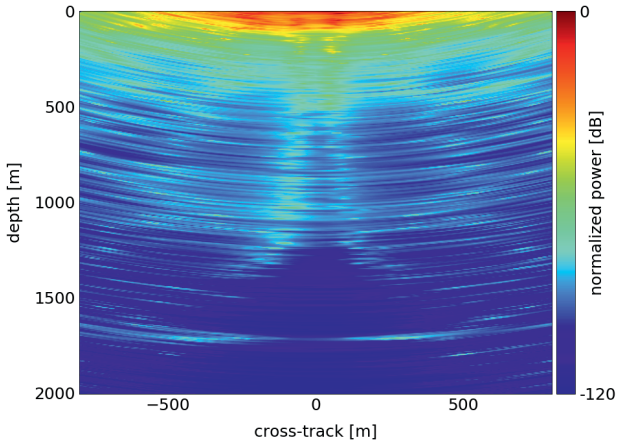

(c) MVDR, B

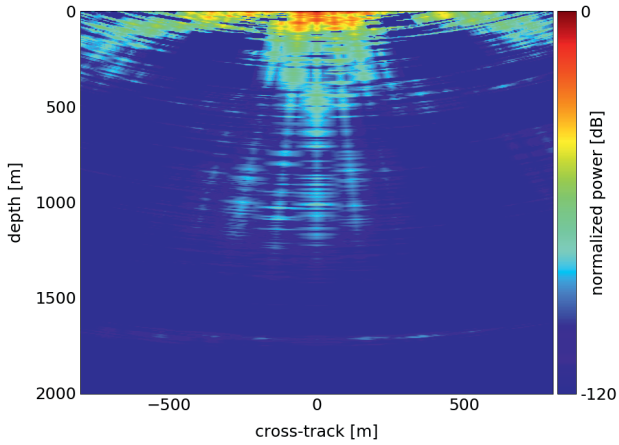

(d) M-FOCUSS, B

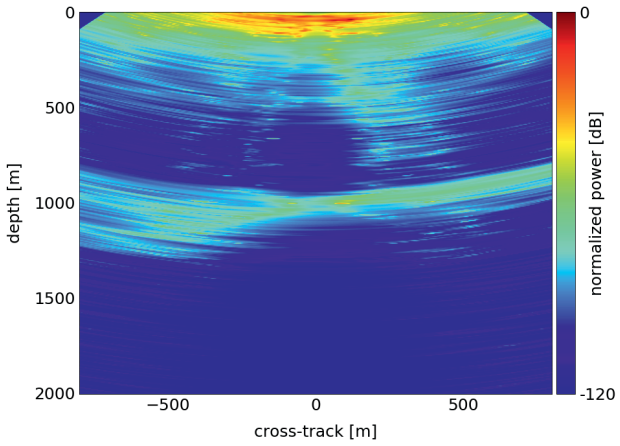

(e) MVDR, C

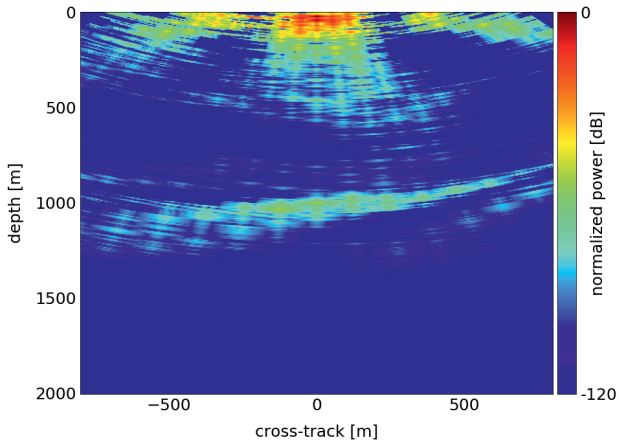

(f) M-FOCUSS, C

Figure 5: Comparison of MVDR and M-FOCUSS cross-track power profiles

ISBN 978-3-8007-4636-1 / ISSN 2197-4403

tribution is clustered around $x \approx 0\,\mathrm{m}$. We attribute the ripple effect observed in the M-FOCUSS profiles, that is mostly pronounced in internal layers, to the non-optimal choice of the sparsifying basis.
Fig. 4 shows maximum intensity projection of volumetric images for both processing techniques. Qualitative comparison of the images suggests that M-FOCUSS provides images of a higher contrast compared to MVDR, as M-FOCUSS by definition performs image de-noising. This fact suggests that M-FOCUSS, being more robust to noise, is a good candidate for processing areas with a hardly detectable bed.

5 Conclusions

We demonstrated 3-D SAR tomography of ice sheet and bed using a sparse signal reconstruction framework. The advantage of sparse reconstruction lies in its ability to work under various range of sampling geometries and also with a limited number of receive channels. The latter is critical in ice sounding applications as it's prohibitively hard to design sensors with large cross-track apertures in the VHF range.

Acknowledgment

We acknowledge the use of data and/or data products from CReSIS generated with support from the University of Kansas, NSF grant ANT-0424589, and NASA Operation IceBridge grant NNX16AH54G.
We also would like to thank John Paden of CReSIS for answering the sensor and data related questions.

References

[1] S. Gogineni, D. Braaten, C. Allen, J. Paden, T. Akins, P. Kanagaratnam, K. Jezek, G. Prescott, G. Jayaraman, V. Ramasami, C. Lewis, and D. Dunson, "Polar radar for ice sheet measurements (PRISM)," *Remote Sensing of Environment*, vol. 111, pp. 204–211, November 2007.

[2] "Recommendations for the collection and synthesis of antarctic ice sheet mass balance data," *Global and Planetary Change*, vol. 42, pp. 1–15, July 2004.

[3] A. Reigber and A. Moreira, "First demonstration of airborne SAR tomography using multibaseline l-band data," *IEEE Transactions on Geoscience and Remote Sensing*, vol. 38, no. 5, pp. 2142–2152, 2000.

[4] X. Wu, K. C. Jezek, E. Rodriguez, S. Gogineni, F. Rodriguez-Morales, and A. Freeman, "Ice sheet bed mapping with airborne SAR tomography," *IEEE Transactions on Geoscience and Remote Sensing*, vol. 49, no. 10 PART 1, pp. 3791–3802, 2011.

[5] A. Heister and R. Scheiber, "First Analysis of Sparse Signal Reconstruction for Radar Imaging of Ice Sheets," in *"Proceedings of EUSAR 2016: 11th European Conference on Synthetic Aperture Radar*, pp. 788–791, VDE, June 2016.

[6] P. Gogineni, "CReSIS radar depth sounder data, Center for Remote Sensing of Ice Sheets, Lawrence, KS, available at: https://data.cresis.ku.edu/," 2012.

[7] E. Candes, J. Romberg, and T. Tao, "Robust uncertainty principles: exact signal reconstruction from highly incomplete frequency information," *IEEE Transactions on Information Theory*, vol. 52, pp. 489–509, feb 2006.

[8] M. Duarte, S. Sarvotham, D. Baron, M. Wakin, and R. Baraniuk, "Distributed compressed sensing of jointly sparse signals," in *Conference Record of the Thirty-Ninth Asilomar Conference on signals, Systems and Computers*, IEEE, 2005.

[9] S. Cotter, B. Rao, K. Engan, and K. Kreutz-Delgado, "Sparse solutions to linear inverse problems with multiple measurement vectors," *IEEE Transactions on Signal Processing*, vol. 53, pp. 2477–2488, July 2005.

[10] A. Rakotomamonjy, "Surveying and comparing simultaneous sparse approximation (or group-lasso) algorithms," *Signal Processing*, vol. 91, pp. 1505–1526, July 2011.

[11] K. Jezek, S. Gogineni, E. Rodriguez, X. Wu, J. Sontag, F. Rodriguez, A. Freeman, and J. Curlander, "Global ice sheet mapping observatory: final report," tech. rep., Earth Science Technology Office, NASA, Greenbelt, MD, USA, January 2009.

